ACS Catalysis

Research Article

pubs.acs.org/acscatalysis

Structural Determinants of Oxidative Stabilization in an Evolved Versatile Peroxidase

David Gonzalez-Perez,[†] Eva Garcia-Ruiz,[‡] Francisco Javier Ruiz-Dueñas,[§] Angel T. Martinez,[§] and Miguel Alcalde*[,†]

[†]Department of Biocatalysis, Institute of Catalysis, CSIC, Marie Curie 2, Cantoblanco, 28049 Madrid, Spain

[‡]Department of Chemical and Biomolecular Engineering, University of Illinois at Urbana−Champaign, 600 South Mathews Avenue, Urbana, Illinois 61801, United States

[§]Biological Research Centre, CSIC, Ramiro de Maeztu 9, 28040 Madrid, Spain

Supporting Information

ABSTRACT: Versatile peroxidases (VP) are promiscuous biocatalysts with the highest fragility to hydroperoxides yet reported due to a complex molecular architecture, with three catalytic sites and several oxidation pathways. To improve the VP resistance to H_2O_2, an evolved version of this enzyme was subjected to a range of directed evolution and hybrid strategies in *Saccharomyces cerevisiae*. After five generations of random, saturation, and domain mutagenesis, together with in vivo DNA recombination, several structural determinants behind the oxidative destabilization of the enzyme were unmasked. To establish a balance between activity and stability, selected beneficial mutations were introduced into novel mutational environments by the in vivo exchange of sequence blocks, promoting epistatic interactions. The best variant of this process accumulated 8 mutations that increased the half-life of the protein from 3 (parental type) to 35 min in the presence of 3000 equiv of H_2O_2 and with a 6 °C upward shift in thermostability. Multiple structural alignment with other H_2O_2-tolerant heme peroxidases help to understand the possible roles played by the new mutations in the overall oxidative stabilization of these enzymes.

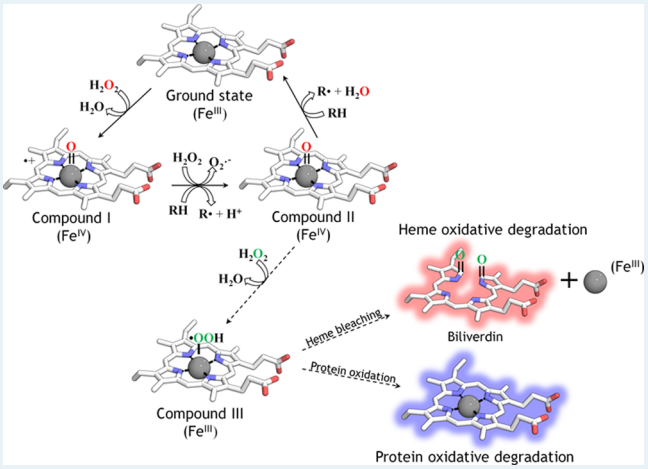

KEYWORDS: *versatile peroxidase, oxidative stability, directed evolution, rational design, Saccharomyces cerevisiae, in vivo DNA recombination*

INTRODUCTION

As well as being quite broadly distributed in nature, peroxidases (EC 1.11.1) are an important group of oxidoreductases that are capable of oxidizing a wide variety of substrates in the presence of peroxides.[1] Heme-containing peroxidases catalyze the successive removal of two electrons from two individual reducing substrates via a *ping-pong* mechanism. In its ferric resting state, the enzyme is activated by H_2O_2 to yield one molecule of water and an oxidized reactive intermediate (an oxoferryl (IV) porphyrin π cation-radical complex, Fe^{IV}=O·$P^{•+}$) called compound I. After the generation of compound I, the first reducing substrate molecule is oxidized so that the enzyme switches to the second catalytic intermediate, called compound II (Fe^{IV}=O), which in turn returns to the ground state (Fe^{III}) after the oxidation of a new reducing substrate and the release of a second water molecule.[2−4]

Although there are many applications for peroxidases, ranging from bioremediation to organic synthesis, their poor oxidative stability in the presence of modest concentrations of H_2O_2 precludes their use in many areas of biotechnology.[5−9] Indeed, for decades, the oxidative damage to peroxidases provoked by H_2O_2 has been considered a hot research topic, given that the complex inhibitory process (referred to as suicide inactivation) is not yet fully understood. This irreversible inactivation occurs either in the presence of the reducing substrate (with an excess of H_2O_2) or in its absence (at catalytic concentrations of H_2O_2), whereby the reaction of compound II with a second peroxide molecule generates compound III, an iron(III) superoxide radical complex that finally fosters inactivation through at least two different pathways: (i) heme bleaching (i.e., protoporphyrin ring cleavage into biliverdin plus Fe^{III}); and/or (ii) protein damage due to the interaction with the reactive oxygen species (ROS) that are generated.[10−13]

Received: August 19, 2014
Revised: September 21, 2014
Published: September 22, 2014

   dx.doi.org/10.1021/cs501218v | *ACS Catal.* 2014, 4, 3891−3901

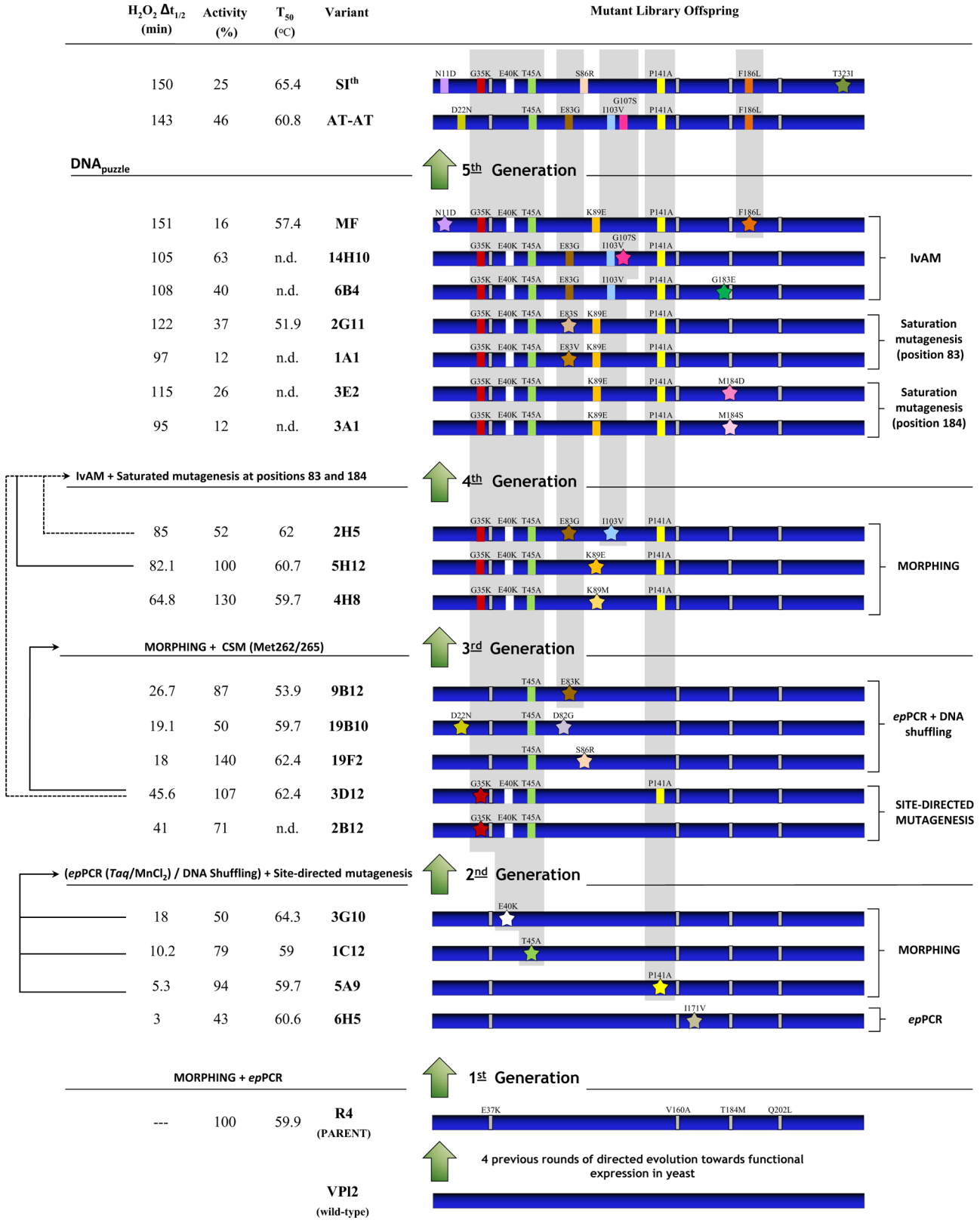

Figure 1. Evolutionary pathway for VP oxidative stability. New mutations are depicted as stars, and accumulated mutation are shown as squares. The amino acid backbone for secretion and activity is indicated by thin gray rectangles. $\Delta t_{1/2}$, the increase in the apparent half-life in the presence of H_2O_2 compared to the R4-parental type calculated from *S. cerevisiae* supernatants. Activity (%), ABTS-activity improvement (given in %) vs the R4-parental type detected in *S. cerevisiae* microcultures. T_{50}, temperature at which the enzyme retains 50% of its activity after a 10 min incubation. MORPHING, mutagenic organized recombination by homologous in vivo grouping; *ep*PCR, error-prone PCR; IvAM, in vivo assembly of mutant libraries; CSM, combinatorial saturation mutagenesis.

dx.doi.org/10.1021/cs501218v | *ACS Catal.* 2014, 4, 3891−3901

Even though some peroxidases are naturally resistant to high concentrations of H_2O_2, unfortunately they are poorly expressed and/or their sequences are not available to perform deeper structure−function studies.[14] To enhance the oxidative stability of heme peroxidases, protein engineering can focus on site-directed mutagenesis to replace the most oxidizable residues (Met, Cys, Trp, His, and Tyr) with lower-redox-potential/less-oxidizable amino acids, as well as performing directed evolution.[15−20] The joint use of these approaches is highly advisable when exploring different intrinsic- and mechanism-based problems, such as the modification of enantio- and stereoselectivity, the creation of novel substrate specificities, or conferring resistance toward different types of inhibitors.[21−23] By contrast, little attention has been paid to the combination of evolutionary and rational/hybrid strategies to engineer H_2O_2 stability in heme peroxidases.

Here, we have used a ligninolytic versatile peroxidase (VP, EC 1.11.1.16) that had been previously evolved in the laboratory for improved expression and activity as the point of departure to tailor oxidative stability.[24] VP are highly promiscuous biocatalysts that share catalytic attributes with lignin peroxidases (LiP), manganese peroxidases (MnP), and generic peroxidases (GP).[25−28] With one of the highest redox potentials found in nature (>+1.4 V), this promiscuous enzyme is capable of oxidizing low-, medium-, and high-redox-potential compounds. Due to a unique structure (with three different catalytic sites and two access channels to the heme domain), VP promiscuity is associated with extreme fragility when confronted by peroxides, making them a challenging model to study suicide inactivation. In the present work, we prepared several strategies that take advantage of the recombination apparatus of *Saccharomyces cerevisiae* to generate DNA diversity and engineer VP, including a *one-pot* random mutagenic method for defined domains, as well as in vivo recombination of a pool of short sequence mutagenized blocks. Enriched mutant libraries with different mutational loads were explored with the help of a sensitive high-throughput screening assay based on an estimated H_2O_2/enzyme molar ratio and the enhanced half-live in the presence of H_2O_2. By combining rational/hybrid and laboratory evolution approaches, several structural determinants involved in oxidative damage were identified. The best VP variants were characterized biochemically and the mutations analyzed by multiple structural alignment in order to shed light on the mechanism underlying oxidative stabilization of heme-peroxidases.

RESULTS AND DISCUSSION

The starting point of this study was the VP from *Pleurotus eryngii* (R4 mutant) that was a product of four generations of directed evolution to improve secretion and activity in the yeast *S. cerevisiae*.[24] The amino acid backbone of the R4 mutant contains the E37K, V160A, T184M, and Q202L mutations that promote the secretion of the enzyme by yeast (∼22 mg/L) in conjunction with an 129-fold improvement in total activity. The K_m for H_2O_2 of the R4 mutant also increased 4-fold, allowing the variant to show high specific activities under saturating conditions. In order to engineer oxidative stability in the R4 mutant, a colorimetric high-throughput screening assay was adjusted for the different mutant libraries constructed in yeast. Because the molar excess of H_2O_2 applied in the screening leads to different responses in function of the activity and secretion of each variant, we carefully chose the H_2O_2/enzyme molar ratio so that the parental types in each generation were capable of maintaining at least 1/3 of their initial activity after a given period in the presence of H_2O_2. Accordingly, the process of evolution was accelerated by progressively enhancing the oxidative stress applied in each generation (up to 0.6 mM of H_2O_2, see Supporting Materials and Methods for details). ABTS (2, 2′-azino-bis(3-ethylbenzothiazoline-6-sulfonic acid)) was used as a reporter, ensuring the screening assay was very reliable with a coefficient of variance ∼12%. Selected clones were subjected to several consecutive rescreenings and in particular, the increase in the apparent half-life in the presence of H_2O_2 compared to the parental type ($\Delta t_{1/2}$) and the kinetic thermostability (based on the T_{50} defined as the temperature at which the enzyme retains 50% of its activity after a 10 min incubation) were both assessed in a third rescreening to rule out the selection of false positives.

Evolutionary and Hybrid Strategy. Approximately 15 000 clones were explored in five generations of laboratory evolution and semirational experiments (Figures 1, S1). Several mutant libraries were constructed in the first round of directed evolution, targeting either the whole VP gene for random mutagenesis or restricting the mutational load to specific regions of 30 to 69 amino acids. The latter approach was performed with the help of an ad hoc domain mutagenesis method known as MORPHING (mutagenic organized recombination process by homologous in vivo grouping) that introduces mutations and promotes recombination in small protein segments.[29] MORPHING took advantage of the high frequency of homologous recombination in *S. cerevisiae*, facilitating the *one-pot* construction of mutant libraries affecting defined regions without altering the remaining parts of the gene.[30] After running multiple structural alignments to identify putative H_2O_2-sensitive regions in VP, the 30 amino acid distal His environment (Leu28-Gly57), the 26 amino acid proximal His environment (Leu149-Ala174), and the 69 amino acid Met environment (Ile199-Leu268) were chosen for MORPHING. The three best variants produced in this generation came from random mutagenesis at the distal and proximal His environments. Given that no beneficial mutations were located in the Met environment, the three oxidizable Met residues in this area (Met247, Met262, and Met265) may not be implicated in the oxidative destabilization of VP (as confirmed by combinatorial saturation mutagenesis, see below). The 3G10 variant (E40K mutation) had a $\Delta t_{1/2}$ of 18 min and a 5 °C improved T_{50} over the parental type, albeit at the cost of a 50% decrease in its activity. By contrast, the 1C12 variant (T45A mutation) had a $\Delta t_{1/2}$ ∼10 min, maintaining ∼80% of its activity and a similar T_{50} as the parental type (∼60 °C). In addition, the 5A9 variant (P141A mutation) had a $\Delta t_{1/2}$ ∼5 min, retaining most of its activity and with the same T_{50} as the parental type.

Taking into account that recombination between the E40K and T45A mutations was very unlikely, second generation double and triple mutants (including P141A) were constructed by site-directed mutagenesis. Both the double and the triple variants (2B12 and 3D12, respectively) incorporated the G35K mutation due to a PCR amplification error, which was conserved during the remaining evolution. The 2B12 and 3D12 variants displayed similar improvements in the $\Delta t_{1/2}$ (ranging from 41 to 46 min) while they retained most of their activity. In parallel, the 3G10, 1C12, and 5A9 mutants from the first generation were randomly mutated and further subjected to in vivo DNA shuffling. From this library, the 9B12 variant (T45A-E83K), 19B10 (D22N-T45A-D82G), and 19F2 (T45A-S86R) were selected, with $\Delta t_{1/2}$'s ranging from 27 to 18 min

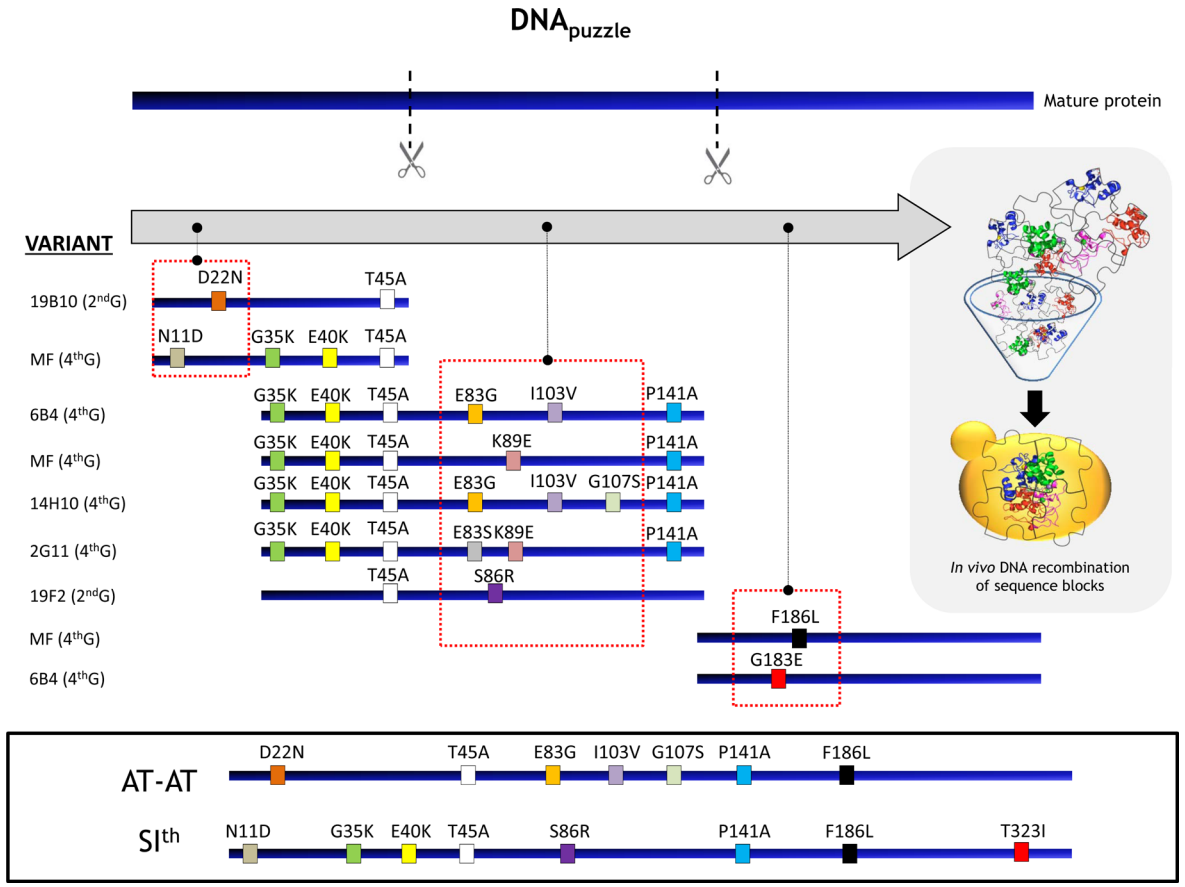

Figure 2. Fifth generation by DNA puzzle. The whole VP fusion gene (including the α-factor prepro-leader for secretion) was fragmented by high fidelity PCR in three independent segments containing overlapping areas flanking each end (the mutations under study are framed with red-dotted lines). The evolved sequence blocks were obtained from different templates from the 2nd and 4th generation. The pool of segments was shuffled and cloned in vivo into *S. cerevisiae* (sequence blocks are represented as pieces of a puzzle). Functional sequences were sorted through the screening assay in terms of $\Delta t_{1/2}$, T_{50}, and total activity values. The T323I mutation of the SIth variant was introduced during the PCR amplification of segment 151−331.

and displaying 50 to 140% of the parental activity. These three variants were exclusive offspring of the 1C12 parental VP (T45A), because the T45A mutation appeared in each, along with the new point mutations underlined. As predicted, crossover events between E40K and T45A did not take place; however, combined site-directed mutagenesis gave us the possibility to assess the effect of these two mutations together.

The best variant of this second generation (3D12) was used as the starting point for a third round of semirational experiments. No improvements were produced when Met262 and Met265 were subjected to combinatorial saturation mutagenesis, confirming the results obtained when the mutant library at the Met environment was explored in the first generation. In fact, ∼95% of the clones in the mutagenic landscapes were inactive, indicating that these positions are highly conserved and they barely tolerate modifications. At this point, it is important to note that three of the four new mutations introduced by mutagenic PCR/DNA shuffling in the second generation were located between positions 82 and 86 (i.e., D82G, E83K, S86R), highlighting the interest in this region for further engineering. Hence, a new library comprising the two helices between residues Gly63-Lys94 (32 amino acids long) was constructed by MORPHING, again mutating Glu83 but this time, to a nonpolar residue (E83G in 2H5 mutant), a position further explored by saturation mutagenesis in generation 4 (see below). Accordingly, two new positions were unmasked: Lys89, with substitutions K89M and K89E in the 4H8 and 5H12 mutants, respectively; and I103V in the 2H5 mutant that was in the overlapping recombination area between fragments. With respect to the parental protein, the new mutants 2H5, 4H8, and 5H12 had a $\Delta t_{1/2}$ from ∼65 to 85 min, retaining 50 to 130% of their activity, and a T_{50} enhanced by 3 °C in the case of 2H5.

In the fourth generation, IvAM (in vivo assembly of mutant libraries[31]) was carried out using 5H12 and 2H5 mutants from the previous round as the parental variants, along with 3D12 from the second round for backcrossing recombination. In this set of experiments, 4H8 was discarded as a parental type due to its reduced thermal and oxidative stability, despite the single mutation at the same position as 5H12 (K89M and K89E for 4H8 and 5H12, respectively). Three new improved variants were identified in this generation (MF, 6B4 and 14H10), the most stable of which was the MF mutant (with a $\Delta t_{1/2}$ = 151 min but a significant decrease in activity) due to the incorporation of two new mutations (N11D and F186L) into 5H12. Moreover, 6B4 and 14H10 (with a $\Delta t_{1/2}$ of 108 and 105 min, respectively) were generated by introducing the G183E and G107S mutations into 2H5, respectively. In parallel, positions 83 and 184 were analyzed individually by saturation mutagenesis of the 5H12 mutant. Glu83 showed mutational redundancy through the second and third generations (i.e., E83K in the 9B12 mutant of the second generation and E83G

dx.doi.org/10.1021/cs501218v | ACS Catal. 2014, 4, 3891−3901

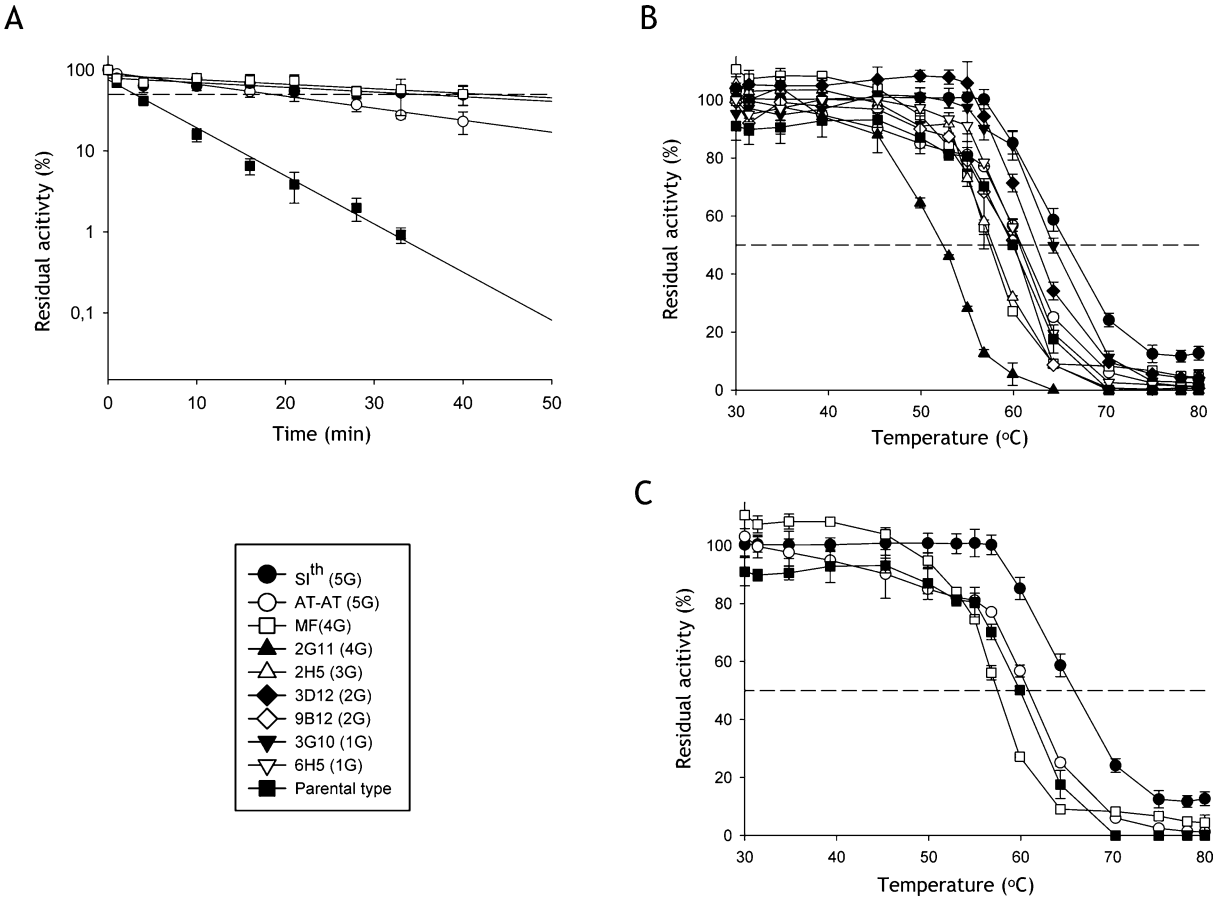

Figure 3. Oxidative and kinetic stabilities. (A) The $t_{1/2}$ H_2O_2. The purified VP samples (1 μM final concentration) were incubated for 90 min in a thermocycler at 25 °C in 100 mM phosphate buffer at pH 6.0 with 3000 equiv of H_2O_2. The residual activity was measured in 100 mM tartrate buffer [pH 3.5] containing 0.1 mM H_2O_2 and 2 mM ABTS. The residual activity refers to the corresponding VP variant incubated in the absence of H_2O_2. H_2O_2 stocks were prepared by measuring absorbance at 240 nm ($\varepsilon_{240}H_2O_2$ = 39.4 M^{-1} cm^{-1}). The protein concentrations of the purified variants were determined at 407 nm using VP extinction coefficient molar (ε_{407} = 150 000 M^{-1} cm^{-1}). The results are the means ± SD for at least three independent experiments. The dashed line indicates 50% of the residual activity. Black squares, R4-parental type; white circles, AT-AT mutant; black circles, SI^{th} mutant; white squares, MF mutant. (B) Kinetic thermostability (T_{50}) for the different VP variants and (C) T_{50} for AT-AT (white circles), SI^{th} (black circles), MF (white squares), and R4 parental type (black squares). The dashed line indicates 50% of the residual activity. The results are the means ± SD of at least three independent experiments.

in the 2H5 mutant of the third generation). On the other hand, Met184 was mutated previously during the directed evolution of VP to favor its functional expression in yeast (T184M).[24] Saturating both positions gave rise to an array of improved variants that contained the E83S, E83V, M184D, and M184S substitutions, yet coupled with an important drop in activity (Figures 1 and S1).

Bringing Balance between Activity and Oxidative Stability through the Exchange of Sequence Blocks in Vivo. The MF mutant obtained in generation 4 was the most stable of all the selected variants in oxidative conditions, yet at the cost of jeopardizing its activity (with a loss of 85% of the parental activity). This trade-off between activity and stability was less pronounced in other variants (e.g., 6B4 and 14H10), which also displayed considerable improvement in oxidative stability. With the aim of drawing a balance between activity and oxidative stability, several mutations were relocated in novel mutational environments by in vivo sequence block exchanges. These experiments aimed to test whether these mutations, which had been ruled out in the course of evolution and/or recombined in specific mutational contexts, could work in new mutational environments to foster epistatic interactions. After revising several domain engineering strategies found in literature,[29,32,33] we decided to prepare a simple method (DNA puzzle) that was supported by yeast homologous recombination. First, we analyzed the whole artificial evolutionary tree to identify suitable sequence blocks, (Figure 1). Most of the mutations were concentrated in distinct independent regions (comprising three segments: α[M1]-S53, C34-L165, and R151-S331) of different variants from generation 2 to generation 4 (Figure 2). Thus, 9 sequence blocks containing the different segments were amplified by high-fidelity PCR from several mutant DNA templates (i.e., 19B10 and 19F2 from generation 2; or MF, 6B4, 14H10 and 2G11 from generation 4). Each individual piece of the DNA puzzle was flanked with 50 bp overhangs to foster the in vivo annealing with each other and with the linearized vector, such that full reassembly of functional sequences could be achieved in a single transformation step in yeast (see Supporting Materials and Methods for details). After screening, the different pieces of the DNA puzzle library were sorted in terms of functionality and H_2O_2 tolerance, such that two improved variants (AT-AT and SI^{th}) were identified. The $\Delta t_{1/2}$ of these two mutants was similar to that of the best variant from generation 4 (the MF mutant), yet with a

dx.doi.org/10.1021/cs501218v | ACS Catal. 2014, 4, 3891−3901

Table 1. Kinetic Parameters for Parental Type and Evolved Variants Expressed in *S. cerevisiae*[a]

substrate	kinetic constants	VPL2[b]	R4-parental type	MF mutant	AT-AT mutant	SIth mutant
ABTS[c]	K_m (mM)	0.54 ± 0.05	0.056 ± 0.003	0.067 ± 0.005	0.095 ± 0.008	0.18 ± 0.02
	k_{cat} (s^{-1})	220 ± 30	365 ± 6	304 ± 7	420 ± 20	400 ± 20
	k_{cat}/K_m (mM^{-1} s^{-1})	410 ± 30	6480 ± 280	4510 ± 260	4400 ± 200	3200 ± 430
DMP[c]	K_m (mM)	32 ± 6	6.5 ± 0.5	48 ± 11	18 ± 3	44 ± 5
	k_{cat} (s^{-1})	98 ± 7	58 ± 1	90 ± 10	110 ± 10	60 ± 4
	k_{cat}/K_m (mM^{-1} s^{-1})	3.1 ± 0.4	9.1 ± 0.5	1.8 ± 0.2	6.0 ± 0.5	1.4 ± 0.07
Mn^{2+}	K_m (mM)	0.045 ± 0.007	0.12 ± 0.01	n.a.	1.1 ± 0.2	n.a.
	k_{cat} (s^{-1})	54 ± 1	75 ± 1	n.a.	140 ± 8	n.a.
	k_{cat}/K_m (mM^{-1} s^{-1})	1190 ± 180	630 ± 50	n.a.	121 ± 15	n.a.
RB5	K_m (mM)	0.007 ± 0.0007	0.0066 ± 0.0004	0.006 ± 0.0007	0.017 ± 0.001	0.004 ± 0.0004
	k_{cat} (s^{-1})	11.8 ± 0.5	10.6 ± 0.2	1.7 ± 0.1	7.6 ± 0.2	2.65 ± 0.06
	k_{cat}/K_m (mM^{-1}. s^{-1})	1670 ± 100	1600 ± 65	250 ± 30	426 ± 17	671 ± 48
H_2O_2-ABTS	K_m (mM)	n.d.	0.15 ± 0.02	0.17 ± 0.01	0.12 ± 0.01	0.12 ± 0.01
	k_{cat} (s^{-1})	n.d.	1120 ± 33	386 ± 6	1036 ± 21	1017 ± 23
	k_{cat}/K_m (mM^{-1} s^{-1})	n.d.	7120 ± 713	2235 ± 105	8230 ± 620	9180 ± 660

[a]VP kinetic constants were estimated in 100 mM sodium tartrate buffer containing 0.1 mM H_2O_2 at pH 3.5 for ABTS, DMP and RB5, and at pH 5.0 for Mn^{2+}. H_2O_2 kinetic constants were measured using ABTS as reducing substrate at the corresponding saturated conditions and taking into account the reaction stoichiometry (one H_2O_2 molecule is reduced for oxidation of two ABTS molecules); n.a. not active; n.d. not determined. [b]Native VPL2 expressed in *S. cerevisiae*. [c]The ABTS and DMP constants correspond to the VP low efficiency site since those for the high efficiency site cannot be measured for R4[24] and the new evolved variants.

noticeable recovery in activity (up to 46% in the AT-AT mutant). Interestingly, only 3 of the 7 mutations in MF were present in the AT-AT mutant, whose sequence blocks came from crossover events between 19B10 (D22N-T45A), 14H10 (E83G-I103V-G107S-P141A), and MF (F186L). The sequence of the SIth mutant was more conserved, with only three different mutations with respect to MF (the suggested crossover events were: N11D-G35K-E40K-T45A from MF, S86R from 19F2, P141A from 6B4/MF/14H10/2G11, and F186L from MF).

Biochemical Characterization. The parental (R4) and mutant (MF [4th generation], AT-AT and SIth [5th generation]) enzymes were purified to homogeneity (Reinheitszahl value: R_z (Abs_{407}/Abs_{280}) ∼ 4) and characterized biochemically. H_2O_2 inhibition can vary strongly depending on the parameters of the assay (i.e., pH, temperature, R_z of the samples, ionic strength and composition of the buffer or the inclusion of different additives).[34−36] We previously compared the oxidative stability of the R4 parental type with that of the native VP heterologously expressed in *Escherichia coli* after in vitro refolding.[24] The poor stability of the VP from *E. coli* led those experiments to be performed in the presence of polyethylene glycol.[37] Here, to better compare the variants secreted by yeast, their half-lives in the presence of H_2O_2 ($t_{1/2}$ H_2O_2) were measured at pH 6.0 and 25 °C in the absence of any additive, and with an excess of 3000 equiv of H_2O_2 (Figure 3A). Under these conditions, the $t_{1/2}$ H_2O_2 for the R4 parental type, MF, SIth and AT-AT were ∼3, 40, 35, and 18 min, respectively, with improvements ranging from 6- to 13-fold. Differences were expected between the apparent $\Delta t_{1/2}$ from the supernatants and the $t_{1/2}$ H_2O_2 obtained from homogeneous purified samples because the H_2O_2/enzyme molar ratio used for screening mutant libraries was based on an estimate of the protein concentration in the culture broth. Nevertheless, a similar tendency in oxidative stability (MF ∼ SIth > AT-AT > R4) was observed when the purified mutants were evaluated, validating our approach.

The kinetic thermostability was measured for the mutant offspring with T_{50} values ranging between ∼14 °C above and below that of the R4 parental type (T_{50} ∼60 °C, Figure 3B). In particular, the T_{50} for the MF, AT-AT and SIth variants were ∼58, 61, and 65 °C, respectively (Figure 3C), the latter representing the strongest improvement in thermostability (5.5 °C above the parental type). This improvement could mostly be attributed to the E40K mutation (a 4.4 °C increase) introduced in the first generation 3G10 mutant and inherited in the SIth mutant (Figure 1).

VP has three different catalytic sites: a Mn^{2+} binding site with three acidic residues implicated in the co-ordination of Mn^{2+} (Glu36, Glu40, and Asp175) that are common to MnP; one catalytic tryptophan residue (Trp164) involved in the oxidation of high-redox-potential compounds through a long-range electron transfer pathway (such as LiP); and the main heme access channel for the oxidation of low and medium-redox-potential substrates (such as GP) although the latter substrates can also be oxidized at the catalytic Trp, as explained below. The kinetic parameters were measured with several substrates that bind to the different catalytic centers of VP. Nonphenolic (ABTS) and phenolic (2, 6 dimethoxyphenol, DMP) substrates are oxidized at the heme access channel (with low efficiency) and at the catalytic tryptophan (with high efficiency), Mn^{2+} is oxidized at the manganese oxidation site and the azo dye Reactive black 5 (RB5) is exclusively oxidized by the catalytic tryptophan (Table 1). The R4 parental type has a 16-fold improved k_{cat}/K_m at the heme channel due to the E37K−V160A−T184M−Q202L amino acid backbone introduced in our previous directed evolution study.[24] Hence, this improvement precluded the evaluation of ABTS or DMP oxidation at the catalytic Trp164, because the kinetics at the heme channel masked their oxidation kinetics at the catalytic tryptophan.

Regardless of the substrate tested, the k_{cat}/K_m values were reduced to a greater or lesser extent, reflecting the delicate balance between the activity and oxidative stability of VP (Table 1). Oxidation at the heme access channel was slightly reduced, showing a general decrease in the substrate's affinity (ranging from a 7.3- to 1.2-fold higher K_m than the R4 parental type) but with a similar (or even enhanced) turnover rate. Still, the kinetics of the mutants in oxidizing ABTS were around 10-

dx.doi.org/10.1021/cs501218v | ACS Catal. 2014, 4, 3891−3901

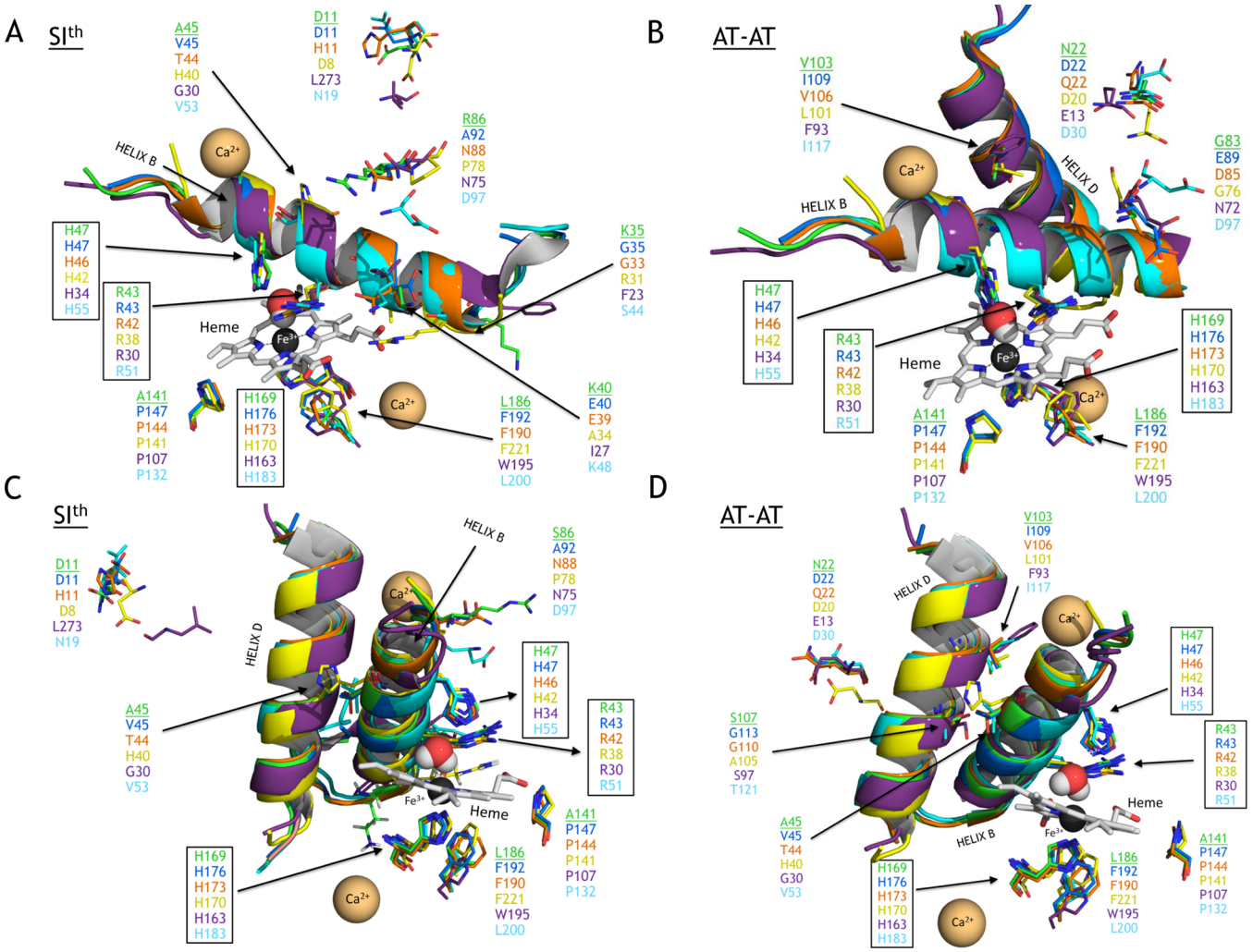

Figure 4. Multiple structural alignment of AT-AT and SIth variants together with several tolerant peroxidases vs H_2O_2. The structure of the wild-type VPL2 (purified from *P. eryngii* culture) at a resolution of 2.8 Å (1 Å = 0.1 nm) (PDB code 3FJW) was used as a template to generate a molecular model in which the newly identified mutations were mapped. The resulting model was analyzed with PyMOL Molecular Visualization System (http://pymol.org). In violet, ApX from *N. tabacum*; in orange MnP isozyme 1 from *P. chrysosporium*; in cyan, CiP from *C. cinerea*; in yellow, HRP isoform C1A from horseradish; in dark blue, LiP isoform H2 from *P. chrysosporium*; in green; VP variants. The structures are shown in cartoon mode and the heme group is highlighted with stick CPK colors, the calcium ions are represented as light-orange spheres, and the water molecule in the active site as red/white spheres. The mutated residues of AT-AT and SIth mutants are underlined and compared with the other peroxidases using a color code (the three Arg43, His47, and His169 residues conserved in all the peroxidases and the evolved variants are also shown, squared). The Ca^{2+} ions and the heme group are shown as the mean of all structures because there may be some differences in the heme or in the structural cations (Ca^{2+} ions being absent from ApX). (A,B), front view; (C,D) side view for SIth and AT-AT, respectively.

fold better than that of the native VPL2 secreted by yeast due to the aforementioned evolved amino acid backbone for total activity. The k_{cat} for RB5 at the catalytic tryptophan notably decreased (from 6- to 1.4-fold depending on the variant), although the affinity for this substrate did not change substantially. The catalytic activity at the Mn^{2+} site was practically quenched after evolution. The MF and SIth variants incorporated the stabilizing E40K mutation (with an improved T_{50} of ∼5 °C, Figure 3B,C) but at the cost of collapsing the Mn^{2+} oxidation site since Glu40 is one of the three coordinating residues of Mn^{2+}. The AT-AT mutant -lacking the E40K substitution- maintained some activity at the Mn^{2+} oxidation site but with a 5-fold lower efficiency than the R4 parental variant. It is worth noting that ABTS was the substrate chosen for the colorimetric assay during screening (a compound easily recognized by both the heme channel site and the catalytic tryptophan residue) and thus, the Mn^{2+} binding pocket was not protected during evolution and its functionality was lost. Indeed, ABTS was employed in the screening when VP was evolved for secretion and activity, jeopardizing the kinetics at the Mn^{2+} due to the E37K mutation in the neighborhood of the Mn^{2+} binding site.[24] The kinetics for H_2O_2 were quite similar to that of the parental type, without further enhancement in the K_m as in the evolved R4 mutant.

Structural Alignment with Other H_2O_2-Tolerant Peroxidases. AT-AT and SIth variants were modeled using the crystal structure of wild VP purified from *P. eryngii* as a template (PDB ID: 3FJW), and they were structurally aligned together with other peroxidases with engineered oxidative stability: chloroplastic ascorbate peroxidase (ApX) from *Nicotiana tabacum*;[38] MnP isozyme 1 from *Phanerochaete chrysosporium*;[20] peroxidase from *Coprinopsis cinerea* (CiP);[17] horseradish peroxidase C1A (HRP);[19] and LiP isoform H2 from *P. chrysosporium*,[39,40] Figure 4. Overall, the protein

dx.doi.org/10.1021/cs501218v | *ACS Catal.* 2014, 4, 3891−3901

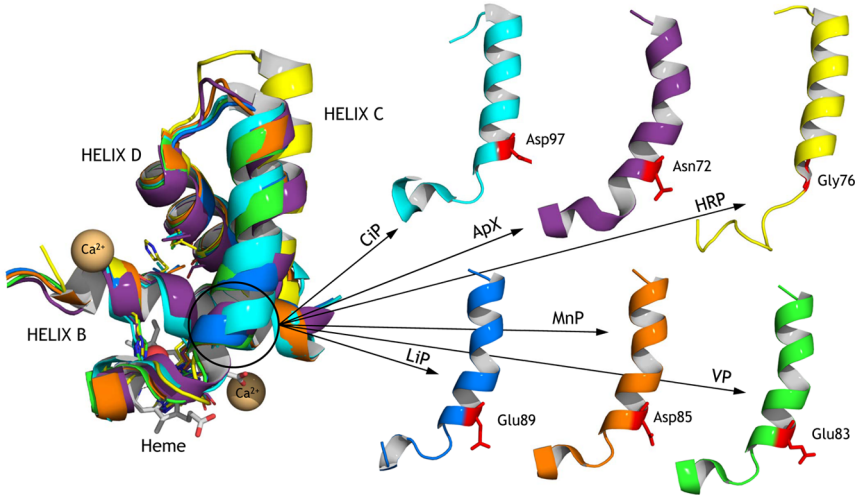

Figure 5. Relative position of VP residue 83 in a multiple structural alignment. VP position 83 (in red-sticks) is shown for the different peroxidases, with modifications in the secondary structure depending on the residue found at this position. The heme group is represented with stick CPK colors and the calcium ions as light-orange spheres. ApX, MnP, CiP, HRP, LiP, and wild-type VP (wtVP).

scaffolds for multiple alignment shared the structural arrangement of typical heme-containing peroxidases generally formed by several alpha helices surrounding the heme prosthetic group and including two structural cations, except in ApX. Following the VP numbering, the main catalytic residues are Arg43 and His47 within helix B (at the heme distal side) and His169 as the fifth Fe^{III}-ligand (at the heme proximal side).

The P141A mutation was located in a loop at the heme entrance, and it is a highly conserved residue among fungal peroxidases. Its replacement by a less bulky residue enlarges the heme access channel, allowing better substrate accommodation near the heme, as described previously for another VP variant at this residue (P141G) with improved affinity for ABTS.[41] Indeed, the P141A substitution also improved the oxidative stability of a VP-thioredoxin fusion protein.[42] The T45A mutation is located at the opposite side of the catalytic amino acids within helix B. This position shows a strong heterogeneity among the peroxidases used in the alignment (i.e., Val, Thr, His, Gly). This region limits the contact between helix D and B, such that the distance between them seems to play a key role in protein function. It is noteworthy that the same substitution was reported in the directed evolution of CiP for H_2O_2 tolerance (V53A using CiP numbering)[17], and hence, we assume that the interactions between both helices are dependent on the size and polarity of these residues. This would affect the relative position of the catalytic His and Arg residues situated in helix B, which are involved in (i) enzyme activation by H_2O_2; (ii) the interaction (directly or through a water molecule) with the ferryl oxygen in compounds I and II; and (iii) the interaction with the superoxide anion in compound III.[43] In relation to the latter, a particularly stable compound III has been associated with the resistance of heme peroxidase from *Raphanus sativus* to H_2O_2.[14] Interestingly, the G107S mutation situated between both helices provoked a strong improvement in oxidative stability and the same position in the evolved CiP was also unmasked.[17] The F186L mutation is located close to the proximal His169 and the same Phe residue was studied in MnP,[44] whereby changes to Ala or Ile reduced stability by up to 2 orders of magnitude. In fact, when the F190A variant was expressed (according to MnP numbering), secretion was reduced up to 90%, whereas the F190W mutation fully inactivated the enzyme. These results suggest that this position plays a critical role in the stability/activity trade-off. LiP, MnP, VP, and HRP contain a Phe residue at the same position, and in ApX this residue is a Trp without any attributed function, whereas the cytochrome C peroxidase has the radical at Trp191.[45−47]

Redundant mutagenesis of the Glu83 residue occurred during the evolution for oxidative stabilization (E83K, second generation; E83G, third generation), and there was an important drop in activity when it was further subjected to saturation mutagenesis (i.e., E83S/V). Glu83 is situated at the end of a loop that connects with the beginning of helix C in VP. Any subtle modification of this residue may vary the interaction with the adjacent helix, giving rise to differences in the length of the secondary structures, as can be deduced from the multiple alignment. Unlike CiP, LiP, MnP, and native VP, which retain a similar secondary organization with acidic residues at this position, HRP and ApX have an Asn and Gly residue, respectively, showing important modifications in the region that connects the loop and the helix (Figure 5). The S86R mutation was located in the middle of helix C, very close to Glu83. This position is not conserved in the other peroxidases (where Ala, Asn, Pro, or Asp residues are found), and according to our models, it may influence the attachment between helix B and D, along with I103V and the aforementioned T45A and G107S mutations. The improvement in the oxidative stability of VP due to mutations in this region was recently suggested by the preliminary analysis of a double mutated variant obtained by simultaneous substitution of the T45 and I103 residues.[48] The E40K and G35K mutations had a negative effect on Mn^{2+} kinetics, suppressing one of the three coordinating acidic residues of the Mn^{2+} sphere and affecting the environment of the binding site. These residues are conserved in MnP, VP, and LiP, yet not in the generic peroxidases as these lack the Mn^{2+} oxidation site. Inactivation of the Mn^{2+} site relaxes the oxidative stress of the enzyme, although at the cost of losing this activity. The T323I mutation (not shown in Figure 4) is placed at the C-terminal end of VP, a region with high mobility that hindered to fix the position of the last 12 residues when the VP crystal structure was determined. We can only speculate about the possible attachment of this mobile region upon mutation to

dx.doi.org/10.1021/cs501218v | *ACS Catal.* 2014, 4, 3891−3901

enhance the stability of the protein. Moreover, although no significant differences were appreciated in the degree of glycosylation (~9%), the T323I mutation might remove the O-glycosylation site seen in the crystal structure of the homologous VP from *P. eryngii* (3FJW). Finally, the N11D and D22N mutations are located at the N-terminal end of the enzyme and they are fairly well conserved in terms of polarity within the other peroxidase scaffolds. Therefore, we cannot find a reasonable explanation as to how these changes affect the oxidative stabilization of VP.

CONCLUSIONS AND OUTLOOK

In the past few years, the mechanism of action of VP has been studied exhaustively, revealing at least three reactive sites (Trp164, main heme access channel, and heme-propionate channel), where electrons can be abstracted from the reducing substrate or from surrounding protein residues in the absence of substrate, in this latter scenario causing oxidative modifications that can lead to enzyme inactivation.[25−27] This phenomenon, which results in the enzyme's self-reduction, together with the generation of ROS related to the formation of compound III in the presence of excess H_2O_2, dramatically lowers the oxidative stability of VP to a few minutes, to the best of our knowledge this being the lowest H_2O_2 stability of all heme-peroxidases reported to date. Here, we have harnessed the recombination apparatus of *S. cerevisiae* to prepare several strategies that induce DNA diversity in order to study the oxidative stability in VP. Some of the structural determinants revealed in this study may be translated to other heme-containing peroxidases, especially those in which mutations are located in highly conserved regions. Nevertheless, the subtle equilibrium between activity and stability is still the biggest hurdle to circumvent. Thus, the use of in silico tools (e.g., quantum mechanics/molecular mechanics) coupled with directed evolution and hybrid approaches may help to tailor novel catalytic functions in this promiscuous biocatalyst. Finally, the appearance of the primitive ancestor of lignin-degrading oxidoreductases was linked to the end of the formation of coal deposits estimated to occur in the Permo-Carboniferous period, ~260 million years ago.[49] Interestingly, the process of in vitro evolution described here defines several stabilizing variants whose functionality at the Mn^{2+} oxidation site was lost, as also happened during the natural evolution transit of VP toward LiP. In the near future, by traveling back and forward in the temporal scale of evolution (using ancestral resurrection and directed evolution tools), we hope to gain more information about the evolutionary history of ligninolytic peroxidases.

MATERIAL AND METHODS

All chemical reagents were of the highest purity commercially available. The oligonucleotides used along the evolutionary process (Supporting Table 1) were purchased from Isogen Life Science (De Meern, The Netherlands). Culture media were prepared as described in the Supporting Material and Methods Section.

Directed Evolution and Hybrid Strategies. For each generation, PCR fragments were cleaned, concentrated, and loaded onto a low melting point preparative agarose gel (Bio-Rad, Hercules, CA), and then purified using the Zymoclean gel DNA recovery kit (Zymo Research, Orange, CA). PCR products were cloned under the control of GAL1 promoter of the pJRoC30 expression shuttle vector (kindly donated by Prof. F. H. Arnold from Caltech, CA), replacing the parent gene in pJRoC30. To remove the parent gene, the pJRoC30 plasmid was linearized with *Bam*HI and *Xho*I (New England Biolabs, Hertfordshire, U.K.), and the linear plasmid was concentrated and purified as described above for the PCR fragments.

Five rounds of directed evolution and hybrid approaches were carried out as described in the Supporting Material and Methods.

High-Throughput Screening (HTS) Protocol. Oxidative stability screening assay was performed as indicated in the Supporting Material and Methods.

Production and Purification of VP Variants. Selected mutants were produced and purified to homogeneity as described in the Supporting Material and Methods.

Biochemical Characterization. *Kinetic Parameters.* Kinetics were assayed with increasing substrate concentrations and fitted to Michaelis−Menten model (steady-state enzyme kinetics) using as template a hyperbolic, single rectangular, and two parameter mode. The catalytic efficiency (k_{cat}/K_m) was obtained plotting turnover rate (s^{-1}) versus substrate concentration and fitting it to a modified hyperbola with function $f(x) = (a.x)/(1 + b.x)$, where (a) is catalytic efficiency and (b) is $1/K_m$. The kinetics were measured with the following enzyme concentrations in a 200 μL final volume: 1.5×10^{-3} μM (ABTS), 1.5×10^{-2} μM (DMP), 2×10^{-2} μM (RB5), 2.5×10^{-4} μM (H_2O_2). Mn^{2+} kinetics were assayed in a final volume of 300 μL in quartz plates (Provair, leatherhead, U.K.) and 2×10^{-2} μM of VP. The following extinction molar coefficients were used: ABTS, $\varepsilon_{418} = 36\,000$ M^{-1} cm^{-1}; DMP, $\varepsilon_{469} = 27\,500$ M^{-1} cm^{-1}; RB5, $\varepsilon_{598} = 50\,000$ M^{-1} cm^{-1}; Mn^{3+}-tartrate, $\varepsilon_{238} = 6500$ M^{-1} cm^{-1}. H_2O_2 kinetics were measured with 2 mM of ABTS. The kinetic parameters were determined in 100 mM tartrate buffer at pH 3.5 for ABTS, DMP, RB5, and H_2O_2, whereas the same buffer at pH 5.0 was employed for Mn^{2+} oxidation.

H_2O_2 Stability Assay. The purified VP samples (1 μM final concentration) were incubated for 90 min in a thermocycler at 25 °C in 100 mM phosphate buffer at pH 6.0 with 3000 equiv of H_2O_2. The residual activity was measured in 100 mM tartrate buffer pH 3.5 containing 0.1 mM H_2O_2 and 2 mM ABTS. The residual activity refers to the corresponding VP variant incubated in the absence of H_2O_2. H_2O_2 stocks were prepared measuring absorbance at 240 nm ($\varepsilon_{240}H_2O_2 = 39.4$ M^{-1} cm^{-1}). The protein concentrations of purified variants were determined at 407 nm using VP molar extinction coefficient ($\varepsilon_{407} = 150\,000$ M^{-1} cm^{-1}).

Thermostability (T_{50}). Appropriate dilutions were prepared such that aliquots (20 μL) produced a linear response in kinetic mode. A gradient profile was constructed using a thermocycler (Mycycler, Bio-Rad, U.S.A.) for the selected mutants and the parental type, using 50 μL for each point in a gradient scale ranging from 30 to 80 °C. After a 10 min incubation, samples were removed and chilled on ice for 10 min. Thereafter, 20 μL of samples were removed and incubated for 5 min at room temperature. Finally, 180 μL of 100 mM sodium tartrate buffer [pH 3.5], 2 mM ABTS, and 0.1 mM H_2O_2 were added to the samples to measure activities. The thermostability values were calculated as the ratio between the residual activity at different temperature points and the initial activity at room temperature. The T_{50} value was determined as the transition midpoint of the inactivation curve of the protein as a function of temperature,

dx.doi.org/10.1021/cs501218v | *ACS Catal.* 2014, 4, 3891−3901

which in our case was defined as the temperature at which the enzyme lost 50% of its initial activity after 10 min of incubation.

Protein and Homology Modeling. The crystal structure of VPL2 from *P. eryngii* at 2.8 Å resolution (1 Å = 0.1 nm, PDB ID: 3FJW) was used to generate a model to map the new mutations found with the help of the PyMOL Molecular Visualization System (Schrödinger). A homology model was generated by carrying out a structural alignment in PyMOL with the following crystal structures (PDB IDs are indicated): 3FJW, native VP from *P. eryngii* was used to model AT-AT and SI^{th} variants; 1IYN, recombinant chloroplastic ApX from *N. tabacum* expressed in *E. coli*; 3M5Q, native MnP isozyme 1 from *P. chrysosporium*; 1H3J, native CiP from *C. cinerea*; 1W4W, recombinant HRP isoform C1A expressed in *E. coli*; and 1LLP, native LiP from *P. chrysosporium*.

■ ASSOCIATED CONTENT

Supporting Information

Additional description of methods used in experiments, diagram and flow chart which show experimental protocol, and table of primers used in this study. This material is available free of charge via the Internet at http://pubs.acs.org.

■ AUTHOR INFORMATION

Corresponding Author

*E-mail: malcalde@icp.csic.es.

Notes

The authors declare no competing financial interest.

■ ACKNOWLEDGMENTS

This work was supported by European Commission Projects (Peroxicats-FP7-KBBE-2010-4-26537; Indox-FP7-KBBE-2013-7-613549; COST-Action CM1303: Systems Biocatalysis) and the National Projects (Evofacel) [BIO2010-19697], (Dewry) [BIO2013-43407-R] and Hipop (BIO2011-26694). F.J.R.-D. is grateful for the award of a "Ramón y Cajal" contract of the Spanish MINECO.

■ REFERENCES

(1) Fawal, N.; Li, Q.; Savelli, B.; Brette, M.; Passaia, G.; Fabre, M.; Mathé, C.; Dunand, C. *Nucleic Acids Res.* **2013**, *41*, 441−444.

(2) Battistuzzi, G.; Bellei, M.; Bortolotti, C. A.; Sola, M. *Arch. Biochem. Biophys.* **2010**, *500*, 21−36.

(3) Poulos, T. L. *Arch. Biochem. Biophys.* **2010**, *500*, 3−12.

(4) Martínez, A. T. In *Industrial Enzymes: Structure, Function and Applications*; Polaina, J., MacCabe, A. P., Eds.; Springer: Berlin, 2007; pp 475−486.

(5) Martínez, A. T.; Ruiz-Dueñas, F. J.; Martínez, M. J.; del Río, J. C.; Gutíerrez, A. *Curr. Opin. Biotechnol.* **2009**, *20*, 348−357.

(6) Gregg, P. K.; Zhao, Y.; Kagan, V. E.; Star, A. *Adv. Drug Delivery Rev.* **2013**, *65*, 1921−1932.

(7) Salvachúa, D.; Prieto, A.; Mattinen, M. L.; Tamminen, T.; Liitiä, T.; Lille, M.; Willför, S.; Martínez, A. T.; Martínez, M. J.; Faulds, C. B. *Enzyme Microb. Technol.* **2013**, *52*, 303−311.

(8) Regalado, C.; García-Almendárez, B. E.; Duarte-Vázquez, M. A. *Phytochem. Rev.* **2004**, *3*, 243−256.

(9) Van de Velde, F.; Lourenço, N. D.; Bakker, M.; van Rantwijk, F.; Sheldon, R. A. *Biotechnol. Bioeng.* **2000**, *69*, 286−291.

(10) Valderrama, B.; Ayala, M.; Vazquez-Duhalt, R. *Chem. Biol.* **2002**, *9*, 555−565.

(11) Ayala, M.; Batista, C. V.; Vazquez-Duhalt, R. *J. Biol. Inorg. Chem.* **2011**, *16*, 63−68.

(12) Hernandez-Ruiz, J.; Arnao, M. B.; Hiner, A. N.; Garcia-Canovas, F.; Acosta, M. *Biochem. J.* **2001**, *354*, 107−114.

(13) Wariishi, H.; Gold, M. H. *FEBS Lett.* **1989**, *243*, 165−168.

(14) Gil-Rodríguez, P.; Ferreira-Batista, C.; Vázquez-Duhalt, R.; Valderrama, B. *Eng. Life Sci.* **2008**, *8*, 286−296.

(15) Ogola, H. J.; Hashimoto, N.; Miyabe, S.; Ashida, H.; Ishikawa, T.; Shibata, H.; Sawa, Y. *Appl. Microbiol. Biotechnol.* **2010**, *87*, 1727−36.

(16) Miyazaki, C.; Takahashi, H. *FEBS Lett.* **2001**, *509*, 111−4.

(17) Cherry, J. R.; Lamsa, M. H.; Schneider, P.; Vind, J.; Svendsen, A.; Jones, A.; Pedersen, A. H. *Nat. Biotechnol.* **1999**, *17*, 379−84.

(18) Cherry, J. R. *Methods Enzymol.* **2004**, *388*, 167−75.

(19) Morawski, B.; Quan, S.; Arnold, F. H. *Biotechnol. Bioeng.* **2001**, *76*, 99−107.

(20) Miyazaki-Imamura, C.; Oohira, K.; Kitagawa, R.; Nakano, H.; Yamane, T.; Takahashi, H. *Method Enzymol.* **2003**, *16*, 423−428.

(21) Mate, D.; Gonzalez-Perez, D.; Falk, M.; Kittl, R.; Pita, M.; De Lacey, A. L.; Ludwig, R.; Shleev, S.; Alcalde, M. *Chem. Biol.* **2013**, *20*, 223−231.

(22) Sun, L.; Bulter, T.; Alcalde, M.; Petrounia, I. P.; Arnold, F. H. *ChemBioChem* **2002**, *3*, 781−783.

(23) Reetz, M. T.; Wang, L. W.; Bocola, M. *Angew. Chem., Int. Ed.* **2006**, *45*, 1236−1241.

(24) Garcia-Ruiz, E.; Gonzalez-Perez, D.; Ruiz-Dueñas, F. J.; Martinez, A. T.; Alcalde, M. *Biochem. J.* **2012**, *441*, 487−498.

(25) Ruiz-Dueñas, F. J.; Martínez, M. J.; Martínez, A. T. *Mol. Microbiol.* **1999**, *31*, 223−235.

(26) Pérez-Boada, M.; Ruiz-Dueñas, F. J.; Pogni, R.; Basosi, R.; Choinowski, T.; Martínez, M. J.; Piontek, K.; Martínez, A. T. *J. Mol. Biol.* **2005**, *354*, 385−402.

(27) Ruiz-Dueñas, F. J.; Morales, M.; García, E.; Miki, Y.; Martínez, M. J.; Martínez, A. T. *J. Exp. Bot.* **2009**, *60*, 441−452.

(28) Garcia-Ruiz, E.; Mate, D. M.; Gonzalez-Perez, D.; Molina-Espeja, P.; Camarero, S.; Martinez, A. T.; Ballesteros, A. O.; Alcalde, M. In *Cascade Biocatalysis*; Riva, S., Fessner, W. D., Eds.; Wiley-VCH Verlag GmbH & Co. KGaA: Weinheim, 2014; pp 1−18.

(29) Gonzalez-Perez, D.; Molina-Espeja, P.; Garcia-Ruiz, E.; Alcalde, M. *PLoS One* **2014**, *9*, e90919.

(30) Gonzalez-Perez, D.; Garcia-Ruiz, E.; Alcalde, M. *Bioeng. Bugs* **2012**, *3*, 172−177.

(31) Zumárraga, M.; Camarero, S.; Shleev, S.; Martínez-Arias, A.; Ballesteros, A.; Plou, F. J.; Alcalde, M. *Proteins* **2008**, *71*, 250−260.

(32) Fasan, R.; Chen, M. M.; Crook, N. C.; Arnold, F. H. *Angew. Chem., Int. Ed.* **2007**, *46*, 8414−8418.

(33) Shivange, A. V.; Marienhagen, J.; Mundhada, H.; Schenk, A.; Schwaneber, U. *Curr. Opin. Chem. Biol.* **2009**, *13*, 19−25.

(34) Böckle, B.; Martínez, M. J.; Guillén, F.; Martínez, A. T. *Appl. Environ. Microb.* **1999**, *65*, 923−928.

(35) Hiner, A. N.; Hernández-Ruiz, J.; Rodríguez-López, J. N.; Arnao, M. B.; Varón, R.; García-Cánovas, F.; Acosta, M. *J. Biol. Inorg. Chem.* **2001**, *6*, 504−516.

(36) Asad, S.; Torabi, S. F.; Fathi-Roudsari, M.; Ghaemi, N.; Khajeh, K. *Int. J. Biol. Macromol.* **2011**, *48*, 566−570.

(37) Mao, L.; Luo, S.; Huang, Q.; Lu, J. *Sci. Rep.* **2013**, *3*, 3126.

(38) Kitajima, S.; Kitamura, M.; Koja, N. *Biochem. Biophys. Res. Commun.* **2008**, *372*, 918−923.

(39) Ryu, K.; Kang, J. H.; Wang, L.; Lee, E. K. *J. Biotechnol.* **2008**, *135*, 241−246.

(40) Ryu, K.; Hwang, S. Y.; Kim, K. H.; Kang, J. H.; Lee, E. K. *J. Biotechnol.* **2008**, *133*, 110−115.

(41) Morales, M.; Mate, M. J.; Romero, A.; Martínez, M. J.; Martínez, A. T.; Ruiz-Dueñas, F. J. *J. Biol. Chem.* **2012**, *287*, 41053−41067.

(42) Bao, X.; Huang, X.; Lu, X.; Li, J. J. *Enzyme Microb. Technol.* **2014**, *54*, 51−58.

(43) Berglund, G. I.; Carlsson, G. H.; Smith, A. T.; Szoke, H.; Henriksen, A.; Hajdu, J. *Nature* **2002**, *417*, 463−468.

(44) Kishi, K.; Hildebrand, D. P.; Kusters-van Someren, M.; Gettemy, J.; Mauk, A. G.; Gold, M. H. *Biochemistry* **1997**, *36*, 4268−4277.

(45) Dolphin, D.; Forman, A.; Borg, D. C.; Fajer, J.; Felton, R. H. *Proc. Natl. Acad. Sci. U.S.A.* **1971**, *68*, 614−618.

(46) Patterson, W. R.; Poulos, T. L.; Goodin, D. B. *Biochemistry* **1995**, *34*, 4342−4345.
(47) Sivaraja, M.; Goodin, D. B.; Smith, M.; Hoffman, B. M. *Science* **1989**, *245*, 738−740.
(48) Saez-Jimenez, V.; Martinez, A. T.; Ruiz-Dueñas, F. J. In *Oxizymes book of abstracts*. Proceedings of OxiZymes Vienna, July 1-4, 2014, Vienna, Austria; Obinger, C., Peterbauer, C., Eds.; Published by University of Natural Resources and Life Sciences: Vienna, Austria, 2014; p152.
(49) Floudas, D.; Binder, M.; Riley, R.; Barry, K.; Blanchette, R. A.; Henrissat, B.; Martínez, A. T.; Otillar, R.; Spatafora, J. W.; Yadav, J. S.; Aerts, A.; Benoit, I.; Boyd, A.; Carlson, A.; Copeland, A.; Coutinho, P. M.; de Vries, R. P.; Ferreira, P.; Findley, K.; Foster, B.; Gaskell, J.; Glotzer, D.; Górecki, P.; Heitman, J.; Hesse, C.; Hori, C.; Igarashi, K.; Jurgens, J. J.; Kallen, N.; Kersten, P.; Kohler, A.; Kües, U.; Kumar, T. K. A.; Kuo, A.; LaButti, K.; Larrondo, L. F.; Lindquist, E.; Ling, A.; Lombard, V.; Lucas, S.; Lundell, T.; Martin, R.; McLaughlin, D. J.; Morgenstern, I.; Morin, E.; Murat, C.; Nagy, L. G.; Nolan, M.; Ohm, R. A.; Patyshakuliyeva, A.; Rokas, A.; Ruiz-Dueñas, F. J.; Sabat, G.; Salamov, A.; Samejima, M.; Schmutz, J.; Slot, J. C.; John, F., St; Stenlid, J.; Sun, H.; Sun, S.; Syed, E.; Tsang, A.; Wiebenga, A.; Young, D.; Pisabarro, A.; Eastwood, D. C.; Martin, F.; Cullen, D.; Grigoriev, I. V.; Hibbett, D. S. *Science* **2012**, *336*, 1715−1719.